# Supporting Information

Li *et al.* 10.1073/pnas.0801390105

## SI Text

**Retinotopy and ROI.** ***Stimuli.*** Wedges and rings made of flickering radial color checker-board patterns were used to identify retinotopic visual areas of each observer. The aspect ratio of the checkers was kept constant by setting their (radial) height equal to their (tangential) mid-width. Four color combinations were used to create the checker-board patterns: black and white, red and cyan, green and purple, and blue and yellow. The display cycled through eight different images per second, consisting of a reversal of each of the four color combinations. The wedge, with an 8.5° radius and a width of one-eighth of a disk, rotated counterclockwise one-fourth of its width per second, so it swept the whole visual field in 32 s. Each ring was made of two checkers in the radial direction. The rings expanded from the center of the display at the speed of one checker per second. The entire cycle took 20 s. The fixation of the display changed from "+" to "×" or vice versa in randomly chosen intervals between 5 and 15 s. ***Procedure.*** In the retinotopy session, observers maintained fixation while viewing rotating wedges, expanding rings, or a flickering annulus. To help them maintain fixation, observers were required to press a key on the MRI-compatible response button box as soon as a change of the fixation mark was detected. A block design was used to measure the retinotopy and the visual cortical regions associated with the stimuli used in the main experiment (regions of interest, ROIs) for each observer before the main experiments. The retinotopy session consisted of one structural MRI run, and two runs of each of the three stimuli: the wedges, the rings, and the annulus used in the main experiment. The wedges and rings allowed us to separate different visual areas.

***Data analysis.*** Gray-white matter segmentation was performed on the 3D structural images for each observer after image intensity inhomogeneity correction and Talairach spatial normalization. The resulting gray-white matter boundaries were used to create a 3D surface model of the brain, which was then inflated to display both sulci and gyri on smooth surfaces. For each hemisphere, a 2D flat cortical map was then created by unfolding the inflated 3D surface around the mid-brain after cutting it in several places, including one along the calcarine sulcus (left edge of cortical sheet in Fig. S1 *b* and *c*). The flat maps involved minimal areal distortions of the 3D data (≈13%).

Polar angle and eccentricity maps were created by (*i*) computing the average fMRI time series of each voxel across multiple wedge and ring runs, (*ii*) calculating the correlation between the measured BOLD time series and the predicted hemodynamic functions (1), and (*iii*) plotting the correlation map ($r > 0.25$) on a flattened representation of visual cortex (Fig. S1*b*). Boundaries between visual areas were delineated using field-sign mapping, which identifies direction reversals of the polar-angle trajectories and is roughly perpendicular to the eccentricity trajectories on the flat visual area maps (2, 3). Manual adjustment was performed when necessary. The retinotopic regions (V1, V2, V3, V3A, and V4) were defined according to the standard convention. For V4, we included the full hemifield (4). Voxels on the retinotopic map that were also activated by the annulus defined the ROI: Subsections of V1, V2, V3, V3A, and V4 (Fig. S1*c*). The corresponding voxels in the fMRI data were used for all of the subsequent ROI analysis.

**Comments on the Attention Manipulation and the Mixed Design.** To maximize the observed effects of attention on the BOLD response, we have chosen a "categorical" manipulation of covert attention. The observed effects of attention may reflect the impact of a mixture of spatial and feature attention. The duration of each block in this mixed-design is 78 s, significantly longer than the typical block duration used in most fMRI experiments. Drift for EPI scans on our scanner is minimal and linear in time and removed in preprocessing steps. We were bounded by the constraints imposed by the demands of counterbalancing (a minimum of 26 trials per block) and BOLD linearity assumption (3 s per trial). The resulting design was a reasonable compromise. The relatively long block duration did not cause any major issues because the trial-by-trial results from the mixed design and the event-related design are virtually the same.

**Model Selection via Nested Model Tests.** Different variants of the Naka-Rushton models were compared using an F-test for nested models. A nested model is one that is a special case of another model in which one of more parameters are equated or fixed. As indicated in the article, the Naka-Rushton equation was fit to the BOLD contrast response functions (CRFs) in each cortical region:

$$R(c) = b + \frac{R_{\max} c^2}{c_{50}^2 + c^2}, \qquad [1]$$

where $c$ is the contrast of the grating, $b$ is the baseline activity, $c_{50}$ denotes the contrast at which the response reaches half of its maximum dynamic range, and $R_{\max}$ is the maximum response above the baseline. For each cortical region, a model is fit simultaneously to the data for the attended and the unattended conditions. In the most saturated model, the attended and unattended condition may differ in all three aspects ($b$, $c_{50}$, and $R_{\max}$) (i.e., two N-R equations with independent estimates of all three parameters). Nested special cases are those in which, for example, the baseline $b$ is assumed to be identical for the attended and unattended condition, and so on. A (nested) reduced model, which is a special case of a fuller model, is tested for significance using the nested $F$ test:

$$F = \frac{(RSS_{\text{reduced}} - RSS_{\text{full}})}{(k_{\text{full}} - k_{\text{reduced}})} \Big/ \frac{(RSS_{\text{full}})}{(k_{\text{full}})},$$

with degrees of freedom $k_{\text{full}} - k_{\text{reduced}}$ and $n - k_{\text{full}}$. The $RSS$ is the residual sum of squared errors for the model (5). The $F$-statistic compares the mean squared errors per each added parameter in the fuller model to the mean squared errors for each remaining degree of freedom after prediction by the fuller model. In other words, the test evaluates whether the variance accounted for by the added parameters in the fuller model is significantly larger than expected by chance. If so, then the added parameter in the fuller model expresses a significant difference between conditions. A lattice of such nested models may be used to identify the model that best accounts for the data with the fewest (significantly different) parameters.

**The Bootstrap Procedure.** To evaluate the effect of individual differences on the model selection results, we conducted a statistical study with the following bootstrap procedure: (*i*) Sampling with replacement the estimated CRFs from six observers. The entire set of CRFs from the five ROIs and attention conditions of each subject was treated as a single unit in the sampling procedure. (*ii*) As with the original data set, the six sets of re-sampled CRFs were averaged, separately for each ROI and

attention conditions and weighted by the standard errors of each BOLD response. (*iii*) The full model lattice based on the modified Naka-Rushton equation was fitted to the average CSFs. (*iv*) The best fitting model, the one that is not significantly different from the most saturated but superior to all its reduced models, was selected. (*v*) Steps *i–iv* were repeated one million times. (*vi*) The frequency of each candidate model as the best fitting model was computed. The standard deviations of the parameters of the baseline plus contrast-gain model were also computed using the bootstrapped samples.

**Eye Movement Results.** The eye-tracking data from two observers were analyzed. Fixation state was quantified along several dimensions: horizontal and vertical eye position during fixation, fixation duration, number of blinks per trial, number of saccades per trial, and saccade amplitude. Only horizontal eye position showed any significant difference between the two attention conditions [$F(1,1) = 422$, $P < 0.05$). The eyes were shifted horizontally away from fixation by an average of 0.13° in the attended (periphery) condition, which was less than 3% of the distance to the inner edge of the grating annulus—too small to be responsible for the observed behavioral or physiological differences between the attended and unattended conditions.

**Effects of Attention at Other Eccentricities.** The aggregated CRFs of the five cortical regions in the attended and unattended were measured at four additional eccentricities: fovea (0–2°), inner annulus 1 (3.6–4.2°), inner annulus 2 (4.2–5°), and an outer annulus (7–7.8°). In fovea, attending to the grating stimulus reduced the BOLD responses from 11.8% to 7.1%, independent of the grating contrast. In inner annuli 1 and 2, the BOLD response didn't depend on grating contrast but was increased by attention. In the outer annulus, the shapes of the BOLD CRFs and the effect of attention are very similar to those in the stimulus annulus.

**The Shape of the BOLD CRFs.** The BOLD CRFs in the early visual areas in the current study exhibited saturation at relatively low signal contrast, particularly in the attended condition. This is consistent with several other event-related BOLD CRF studies using brief stimuli (6, 7). In contrast, BOLD CRFs in several block-design studies showed either little saturation or saturation in much higher signal contrasts (8–10). The saturation points in the event-related and block designs may differ due to the different stimulus durations, contrast adaptation levels, and perhaps attentional states.


1. Boynton GM, Demb JB, Heeger DJ (1996) Neural basis of contrast appearance measured with fMRI. *Invest Ophthalmol Visual Sci* 37:4210–4210.
2. Engel SA, Glover GH, Wandell BA (1997) Retinotopic organization in human visual cortex and the spatial precision of functional MRI. *Cereb Cortex* 7:181–192.
3. Sereno MI, *et al.* (1995) Borders of multiple visual areas in humans revealed by functional magnetic-resonance-imaging. *Science* 268:889–893.
4. Wandell BA, Brewer AA, Dougherty RF (2005) Visual field map clusters in human cortex. *Philos Trans R Soc London Ser B* 360:693–707.
5. Wonnacott TH, Wonnacott RJ (1981) *Regression: A Second Course in Statistics* (Wiley, New York).
6. Gardner JL, *et al.* (2005) Contrast adaptation and representation in human early visual cortex. *Neuron* 47:607–620.
7. Murray SO, He S (2006) Contrast invariance in the human lateral occipital complex depends on attention. *Curr Biol* 16:606–611.
8. Avidan G, *et al.* (2002) Contrast sensitivity in human visual areas and its relationship to object recognition. *J Neurophysiol* 87:3102.
9. Boynton GM, Demb JB, Glover GH, Heeger DJ (1999) Neuronal basis of contrast discrimination. *Vision Res* 39:257–269.
10. Olman CA, Ugurbil K, Schrater P, Kersten D (2004) BOLD fMRI and psychophysical measurements of contrast response to broadband images. *Vision Res* 44:669–683.

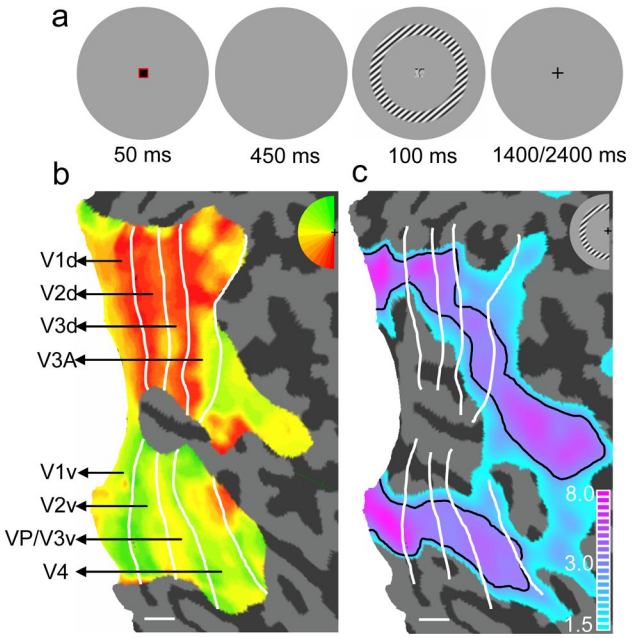


**Fig. S1.** Stimulus and regions of interest. (*a*) Display sequence of a typical trial. (*b*) The retinotopy of a typical subject. The colors denote significant activations by the wedge stimulus in the different sectors of the visual field, as illustrated by the half-disk at the upper right corner. (*c*) Regions of interest, demarcated by the black lines ($t \geq 3$, $P < 0.003$) and boundaries of visual areas (the white lines). Different $t$ values are illustrated using different colors. (Scale bars: 1 cm on the flattened cortical surface.)